Frequency Regulation in Smart Microgrids Based on Load Estimation

(article starts on next page)

SBA

CrossMark

Frequency Regulation in Smart Microgrids Based on Load Estimation

Alexander Stotsky[1]

Abstract

The desired frequency is maintained in Smart Microgrid (SMG) when the generated power matches the grid load. Variability of wind power and fluctuations of the load are the main obstacles for performance improvement of frequency regulation in SMG. Active Power Control (APC) services provided by wind power generators is one of the main sources for performance improvement in frequency regulation. New coordinated APC architecture, which involves simultaneous speed and pitch control actions delivers desired power to the grid despite significant variations of the wind power. A tool-kit with discrete-time input estimation algorithms, which estimate input quantity using output measurements is presented. Unmeasurable load fluctuations are estimated with input estimation method using measurements of grid frequency deviation. Desired power for APC is driven by estimated and a priori known loads. This observer-based control method reduces the risk of overshoots and oscillations in frequency regulation loop compared to PID controllers driven directly by the frequency deviation. The stability of the closed loop frequency control system is proved, and simulation results show that observer-based control architecture provides significant improvement of the frequency regulation in SMG.

1 Introduction

Traditional load frequency control concepts, which are suitable for large centralized power generation, are not suitable for power systems with small decentralized renewable generation units in microgrids due to the lack of large inertias. Frequency control challenges can be addressed within the concept of future Smart Microgrid (SMG), which is a small-scale version of the centralized electricity system (Farhangi 2010). SMG includes interconnection of power generators such as wind turbines, PV units and others; storage devices such as energy capacitors, batteries and others; loads (both uncontrollable and controllable); communication channels and control units, see Fig. 1 for benchmark SMG architecture.

SMG has a number of benefits: (a) power is generated and consumed locally (for islanded operation), and transmission losses are reduced; (b) daily load profiles are usually well known for microgrids and can be used as a priory infor-

mation for frequency control systems; (c) information from smart sensors (which measure frequency deviations, power disturbances and other quantities) transmitted via local communication system with minimal delay can also be used for active control of power generators; (c) and many others. Variability and uncertainty associated with (a) renewable energy sources, such as wind and solar power; (b) load fluctuations due to changing weather conditions, temperature, humidity, economic factors like energy prices, disturbances from the utility grid and others can significantly challenge the performance of SMG. These disturbances usually result in voltage and frequency variations (since the desired grid frequency is maintained when the generated power matches the grid load) in microgrids.

A number of known frequency control schemes in SMG is based on the idea of compensation of power and load deviations with energy storage, see Fig. 1. This solution is expensive and ineffective when power fluctuations exceed the capacity of the power banks. Another idea of load shedding for minimizing frequency deviations has a significant impact on the overall system operation and performance of microgrids. Moreover, load side control requires installation

✉ Alexander Stotsky
   alexander.stotsky@telia.com

[1] Department of Electric Power Engineering, Chalmers
   University of Technology, 412 96 Gothenburg, Sweden

🙋 Springer

of additional expensive hardware and has limited regulation performance.

Notice that wind power plants may actively participate in the frequency regulation via Active Power Control (APC) (Undrill 2010; Aho 2012; Wang-Hansen et al. 2012; Fleming 2016). Nevertheless, unpredictable load fluctuations and variability of the wind, which is the main power source, are again the major obstacles for the high-performance wind turbine APC. However, these challenges can be addressed on the wind turbine control system level (without installation of additional hardware), which provides more efficient solution.

This paper addresses an important issue of high-performance frequency regulation in SMG via wind turbine APC in the presence of unknown load fluctuations.

Notice that APC service from wind turbine may participate in the grid frequency regulation together with other energy sources such as diesel generators, PV units, power banks, load side control units and others. The signal of the frequency in SMG is available in the central control unit, see Fig. 1, which calculates total desired generated power required for minimization of the frequency deviation. The total requested power is distributed by the control unit (taking into account environmental conditions, like wind speed, sunlight and others) by sending appropriate commands to power generators.

Maximization of power production, which is a traditional strategy for turbine control systems, is not directly applicable for APC. To achieve the desired turbine power two approaches can be applied : pitch and torque control, see Aho (2012), Wang-Hansen et al. (2012), Fleming (2016), Yingcheng and Nengling (2011), Pao and Johnson (2009) and references therein. The former reduces the rated speed of the turbine and initiates pitch control at a lower power, providing power reserve for frequency regulation. The latter provides turbine operation govern by torque controller on a suboptimal tip-speed ratio, again providing power reserve. Notice that both loops can control turbine power and operate approximately at the same frequency range. Straightforward application of both control loops to turbine power control may result in suboptimal or conflicting (and even unstable) regulation.

This paper provides new and easy-to-implement control architecture for APC in SMG, driven by estimated load, which combines pitch and torque control. Turbine pitch controller is used as a main tool for turbine power control and torque control loop maximizes the turbine power along the trajectory of turbine pitch angle. Conflicting regulation is absolutely excluded in this scheme due to proper coordination of the control loops. Moreover, this observer-based control method reduces the risk of overshoots and oscillations in the frequency regulation loop due to accurate estimation of the load (since the controller asks for desired power, which matches exactly grid load), compared to other control

schemes (PID controls for example), driven directly by the frequency deviation (Wang-Hansen et al. 2012; Yingcheng and Nengling 2011). These controllers may provide high-gain frequency control actions, which result in frequency overshoots and even oscillations.

The stability of proposed closed loop frequency control system is proved, and simulation results show that the observer-based control architecture provides significant improvement of the frequency regulation in microgrid.

Moreover, a tool-kit associated with input estimation algorithms is proposed in this paper for estimation of unknown load fluctuations using measurements of the frequency deviation only.

2 Wind Turbine Power and Grid Frequency Modeling

2.1 Turbine Power Modeling

The wind turbine converts energy from the wind to the rotor shaft that rotates at a speed ω, (Pao and Johnson 2009). The power of the wind $P_{\text{wind}} = \frac{1}{2}\rho A V^3$ depends on the wind speed V, the air density ρ, and the swept area $A = \pi R^2$, where R is the rotor radius. From the available power in the swept area, the power on the rotor P is given based on the power coefficient $C_{\text{p}}(\lambda, \beta) = \frac{P}{P_{\text{wind}}}$, which in turn depends on the pitch angle of the blades β and the tip-speed ratio $\lambda = \frac{\omega R}{V}$:

$$P = P_{\text{wind}} \, C_{\text{p}}(\lambda, \beta) = \frac{A\rho V^3 C_{\text{p}}(\lambda, \beta)}{2} \qquad (1)$$

Simplified model for blade pitch angle with rate and range constraints and for turbine speed can be presented as follows:

$$\dot{\beta} = -\frac{1}{\tau}\beta + \frac{1}{\tau}\beta_{\text{d}}, \quad 0 \le \beta \le \beta_{\text{m}}, \ |\dot{\beta}| \le C_{\dot{\beta}} \qquad (2)$$

$$J\dot{\omega} = \frac{P}{N\omega} - T_{\text{g}} \qquad (3)$$

where τ is pitch actuator time constant, β_{m} is maximal angle for pitch actuation, $C_{\dot{\beta}}$ is constant associated with the rate constraint, J is lumped rotational inertia, N is gear ratio, and T_{g} is generator torque.

2.2 Model of the Frequency Deviation in the Grid

The deviation from nominal frequency in microgrid can be described by well-known swing equation (Berkel 2013):
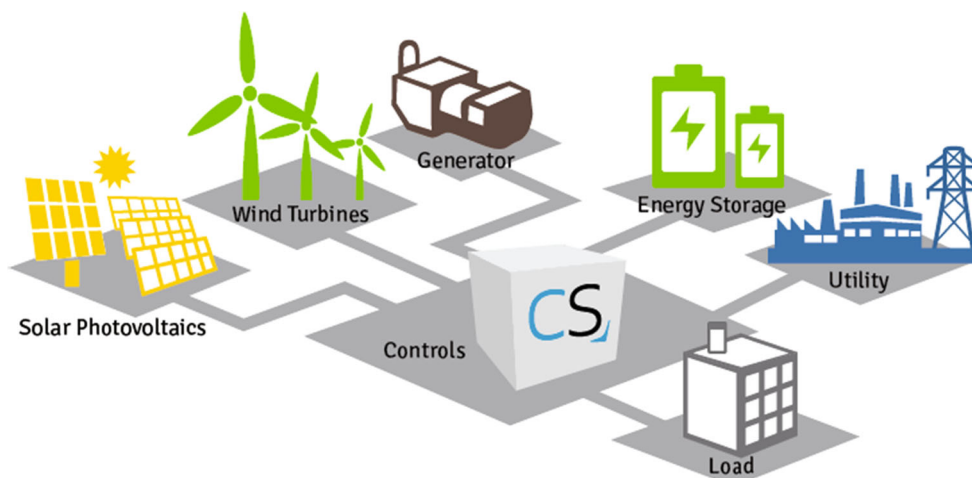
$$\Delta\dot{f} = -a_g \Delta f + b_g(P_{\text{s}} - P_{\text{l}}) \qquad (4)$$

Fig. 1 Benchmark microgrid topology

where Δf is the frequency deviation, $P_{\mathrm{s}} = P_{\mathrm{g}} - P_{\mathrm{la}}$ is a difference between generated power P_{g} and a priory known load P_{la}, and P_{l} is unknown load. The parameters a_g and b_g in (4) are positive and depend on SMG topology.

Detailed modeling of the inertial response of microgrid, derivation of aggregated swing equation and definition of the parameters a_g and b_g are presented for example in Ulbig et al. (2014) and Fan (2017).

The frequency deviation Δf in (4) is controlled via generated power P_{g}. Known load P_{la} [which can also be seen as a feedforward part of the model (4)] represents integrated consumption profile of different customers (industrial and residential) in SMG (Pipattanasomporn 2014). The shape of this curve is associated with daily and weekly periodicity. This profile is modified from day to day and from week to week, taking into account changes in consumption, weather conditions and others. Typically, daily load profiles are classified into week days and weekend days. Four normalized load profiles[1] for week days are presented in Fig. 2. Known load profile can even be used for load forecast (together with weather forecast) to enhance the performance of frequency regulation.

Unknown load profile P_{l} represents unpredictable part and includes all the variations, which are not modeled in the known load profile P_{la}. This component consists usually of two parts: slowly varying component associated with the errors in estimation of known load profile P_{la}, and random component due to accidental causes.

Notice that in addition to wind turbine many energy sources can contribute to the generated power P_{g}, and hence to frequency regulation in SMG, see Fig. 1. The frequency signal is available in the central control unit, which distributes
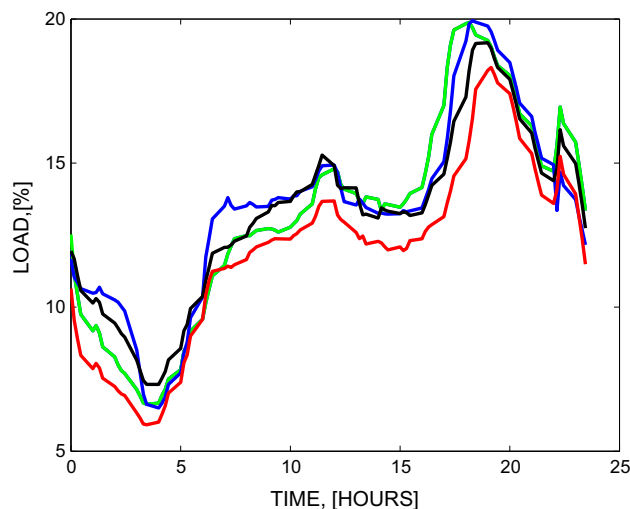

Fig. 2 Microgrid load profiles for four week days

the power required for minimization of the frequency deviation Δf among power generators.

For the sake of simplicity, but without loss of generality, it is assumed that the turbine power is sufficiently large for participation of the wind turbine only (without other power generators) in the frequency regulation.

2.3 Problem Statement: Frequency Regulation

The problem is to find two turbine control variables (a) generator torque T_{g} and (b) blade pitch angle β_{d} to regulate the frequency deviation Δf so that:

$$\lim_{t \to \infty} \Delta f = 0 \tag{5}$$

in the presence of unknown load P_{l} in SMG.

---

[1] https://www.uez.de/Lastprofile.html.

3 Active Power Control via Pitch Regulation with Maximization of Turbine Power

3.1 Problem Statement: Active Power Control

The frequency regulation control aim (5) can be achieved via a proper choice of desired turbine power P_d and APC service, which regulates the turbine power P to the desired power P_d. The turbine power P in turn can be controlled via turbine speed and blade pitch angle. Therefore, the aim (5) can be developed in two main control aims (6) and (7):

$$\lim_{t \to \infty} \beta - \beta_d = 0 \tag{6}$$

$$\lim_{t \to \infty} \omega - \omega_d = 0 \tag{7}$$

$$\lim_{t \to \infty} P - P_d = 0 \tag{8}$$

which correspond to pitch and speed regulation, respectively, with desired trajectories β_d and ω_d, and the secondary aim (8) whose achievement is associated with achievement of the main aims.

3.2 Simplification of Nonlinear Turbine Model for APC

Simplification of (1) for control purposes is necessary due to highly nonlinear relation between the turbine power P and turbine speed and pitch angle.

Define (a) optimal tip-speed ratio $\lambda_*(\beta)$ as a function of a pitch angle, see Fig. 3, and (b) optimal turbine speed ω_* as a function of optimal tip-speed ratio and wind speed that maximize power output as follows:

$$\lambda_*(\beta) = \max_{\lambda} C_p(\lambda, \beta) \tag{9}$$

$$\omega_* = \frac{\lambda_*(\beta)V}{R} \tag{10}$$

Relations (9), (10) can be seen as a constraint that reduces the number of independent variables. Indeed, Fig. 3 shows that $\lambda_*(\beta)$ and ω_* define trajectories as a function of one independent variable β only for a fixed wind speed.

Assume that the turbine speed is controlled via generator torque T_g and deviation between actual turbine speed and desired one are minor i.e., $\omega \approx \omega_*$ and $\lambda \approx \lambda_*$ for any blade pitch angle β. In other words, the turbine is operating around optimal trajectory $\lambda_*(\beta)$, see Fig. 3, and this operation is guaranteed by the turbine speed controller. This assumption is reasonable and verified with measurement data, see for example Figure 5 in Stotsky (2014).

Then, the turbine power can be presented as a function of two independent variables only V and β for a given air
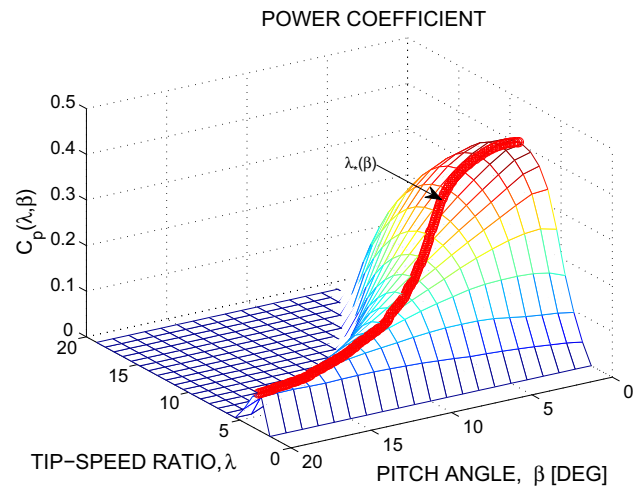

Fig. 3 Optimal tip-speed ratio $\lambda_*(\beta) = \max_{\lambda} C_p(\lambda, \beta)$, plotted with a red line is a function of a pitch angle β
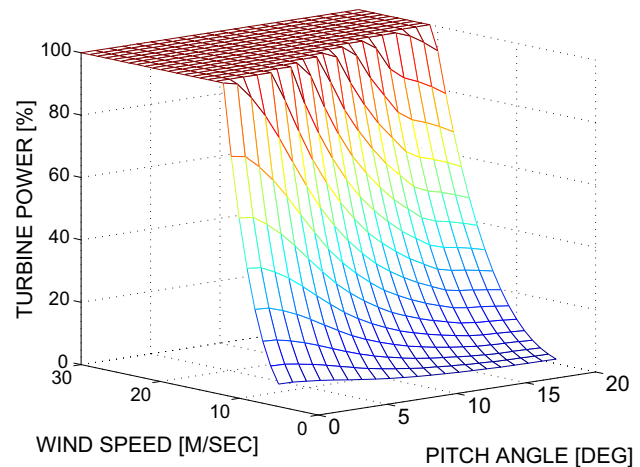

Fig. 4 Normalized turbine power surface as a function of wind speed and blade pitch angle, $P = \frac{A\rho V^3 C_p(\lambda_*(\beta), \beta)}{2} = f(V, \beta)$

density:

$$P = \frac{A\rho V^3 C_p(\lambda_*(\beta), \beta)}{2} = f(V, \beta) \tag{11}$$

which shows that the turbine power can be controlled via blade pitch angle only. Normalized turbine power surface as function of wind speed and blade pitch angle is plotted in Fig. 4.

Introducing inverse function f^{-1}, the pitch angle can be defined as $\beta = f^{-1}(V, P)$, see Fig. 5, such that $P = f(V, \beta) = f(V, f^{-1}(V, P)) = P$.

Then the turbine power can be controlled via blade pitch angle as follows:

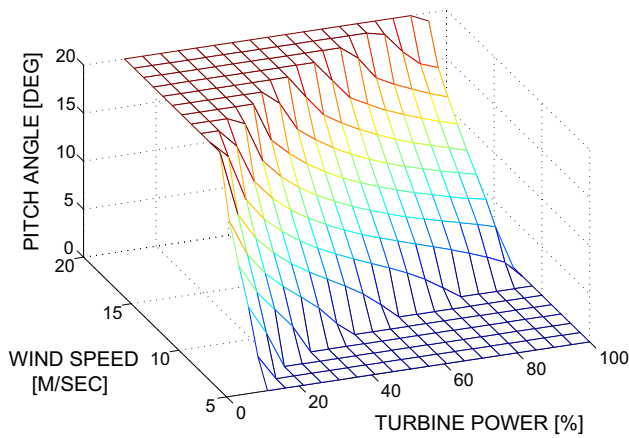$$\beta_d = f^{-1}(V, P_d) \tag{12}$$

Fig. 5 Inverse surface $\beta = f^{-1}(V, P)$, where pitch angle is a function of wind speed and turbine power

where P_d is the desired turbine power, which belongs to some admissible region.

The turbine may provide requested power P_d, if the range constraints (2) for requested pitch angle β_d are not violated at a given wind speed. Preview wind speed information (provided by the LIDAR) and load preview (provided by a priory load profile, see Fig. 2, and/or by load measurement system) may be used for prediction of desired pitch profile and verification of power provision on a short time scale.

Figure 5 shows that the turbine power is controllable via blade pitch angle in a given wind speed range.

3.3 Calculation of Desired Trajectories nd Coordination of Speed and Pitch Control Loops

The chain of calculations of desired trajectories starts with calculation of the desired pitch angle trajectory β_d using relation (12) with desired power profile and wind speed as input variables. Then desired turbine speed profile is calculated according to the following relation:

$$\omega_d = \frac{\lambda_*(\beta_d)V}{R} \tag{13}$$

where $\lambda_*(\cdot)$ is defined in Fig. 3.

Taylor series expansion of the power coefficient $C_p(\lambda, \beta)$ around operating points $\lambda_d = \dfrac{\omega_d R}{V}$ and β_d yields:

$$P = \underbrace{\frac{A\rho V^3 C_p(\lambda, \beta)}{2}}_{\text{actual power}} = \underbrace{P_d}_{\text{desired power}} + \frac{A\rho V^3}{2}$$

$$\left\{ C_{p\beta}(\lambda_d, \beta_d)(\beta - \beta_d) + \frac{1}{2} \left[C_{p\lambda\lambda}(\lambda_d, \beta_d)(\lambda - \lambda_d)^2 \right.\right.$$

$$+ 2\, C_{p\lambda\beta}(\lambda_d, \beta_d)(\lambda - \lambda_d)(\beta - \beta_d)$$

$$+ C_{p\beta\beta}(\lambda_d, \beta_d)(\beta - \beta_d)^2 \bigg]$$

$$+ \cdots + \text{high order terms} \bigg\} \tag{14}$$

where $P_d = \dfrac{A\rho V^3 C_p(\lambda_d, \beta_d)}{2}$ is the desired power, and $C_{p\lambda}(\cdot)$ and $C_{p\beta}(\cdot)$ are partial derivatives of the power coefficient with respect to λ and β respectively.

Equation (14) shows that the convergence of the turbine power P to the desired power P_d can be achieved if the terms in braces are vanishing terms, which means that the tip-speed ratio and pitch angle converge to the desired values. In other words the achievement of the control aim (8) follows immediately from the achievement of the aims (6) and (7).

4 Estimation of Unknown Load

Calculation of the desired turbine power P_d is impossible without knowing grid load, which contains unknown component P_l. Unknown load P_l can be recovered using measurements of the frequency deviation. The load is more convenient to estimate in discrete-time domain, taking into account discrete nature of the frequency measurements. Discretization of Eq. (4) yields:

$$\Delta f_k = a\Delta f_{k-1} + (P_{sk-1} - P_{lk-1}) + \xi_{k-1} \tag{15}$$

where Δf_k is measured frequency deviation, $0 < a < 1$, ξ_k is the load measurement noise, $k = 1, 2, \ldots$.

Algorithm (27) described in Appendix 1 can be applied for estimation of unknown load in the model (15) as follows:

$$\hat{P}_{lk} = \left\{ a^k \Delta f_0 + \sum_{j=0}^{k-1} a^{k-j-1} P_{sj} - \Delta f_k \right\} \frac{(1-a)}{(1-a^k)} \tag{16}$$

Observer (16) estimates the mismatch between generated power P_g and a priory known load P_{la} (both variables are included in the observer) using measurements of the frequency deviation Δf_k.

Introduction of this observer in the control loop is similar in some sense to introduction of the integral term, which compensates for unknown, but constant disturbances. Observer-based frequency control schemes, which take into account the topology of microgrid provide better performance compared to integral terms in the controllers, which are difficult to calibrate for all the working points.

Notice that load estimation performance can be improved in some cases when applying other types of observers, described for example in Appendix 1.

Notice also that reliable frequency measurements are necessary for high-performance frequency control as well as for

system protection. Errors in frequency measurements will result in erroneous control action and even in frequency oscillations. Fast frequency variations and uncertainties associated with unknown harmonics are the main obstacles to performance improvement of frequency estimation with classical zero crossing method. A novel grid frequency estimation method based on multiple model, which overcomes these difficulties, was proposed recently in Stotsky (2016a).

5 Summary of the Frequency Control Strategy, Stability Analysis and Simulation Results

Simple and easy-to-implement observer-based frequency control strategy can be summarized as follows:

$$\hat{P}_{lk} = \left\{ a^k \Delta f_0 + \sum_{j=0}^{k-1} a^{k-j-1} P_{sj} - \Delta f_k \right\} \frac{(1-a)}{(1-a^k)} \quad (17)$$

$$P_{\mathrm{d}} = P_{\mathrm{la}} + \hat{P}_{\mathrm{l}} \quad (18)$$

$$\beta_{\mathrm{d}} = f^{-1}(V, P_{\mathrm{d}}) \quad (19)$$

$$\omega_{\mathrm{d}} = \frac{\lambda_*(\beta_{\mathrm{d}})V}{R} \quad (20)$$

$$T_{\mathrm{g}} = \frac{P}{N\omega_{\mathrm{d}}} \quad (21)$$

The strategy starts with estimation of unknown load P_{l} in discrete time, using frequency deviation Δf, see equation (17). Estimated load $\hat{P}_{\mathrm{l}}$ together with a priory known load P_{la} forms the turbine power request P_{d} in (18). Set-points for blade pitch angle and turbine speed are defined in (19) (see also Fig. 5) and (20), respectively. Finally, generator torque control action is defined in (21).

Substitution of (19), (20) and (18) in (2), (3), and (14), respectively, results in the error model (22) - (24). The error equation (25) is obtained via substitution of (17) and (18) in (4).

Finally, the error model can be summarized as follows:

$$\dot{\tilde{\beta}} = -\frac{1}{\tau} \tilde{\beta} \quad (22)$$

$$J\dot{\tilde{\omega}} = -\frac{P}{N\omega\omega_{\mathrm{d}}} \tilde{\omega} \quad (23)$$

$$\tilde{P} = \frac{A\rho V^3}{2} \left\{ C_{p\beta}(\lambda_{\mathrm{d}}, \beta_{\mathrm{d}})\tilde{\beta} + \frac{1}{2} \left[\frac{R^2}{V^2} C_{p\lambda\lambda}(\lambda_{\mathrm{d}}, \beta_{\mathrm{d}})\tilde{\omega}^2 \right. \right.$$

$$\left. + \frac{2R}{V} C_{p\lambda\beta}(\lambda_{\mathrm{d}}, \beta_{\mathrm{d}})\tilde{\omega}\tilde{\beta} + C_{p\beta\beta}(\lambda_{\mathrm{d}}, \beta_{\mathrm{d}})\tilde{\beta}^2 \right]$$

$$\left. + \cdots + \text{high order terms} \right\} \quad (24)$$

$$\Delta\dot{f} = -a_g \Delta f + b_g \tilde{P} + \varepsilon_t \quad (25)$$

where $\tilde{\beta} = \beta - \beta_{\mathrm{d}}, \tilde{\omega} = \omega - \omega_{\mathrm{d}}, \lambda - \lambda_{\mathrm{d}} = \frac{R}{V}\tilde{\omega}, \tilde{P} = P - P_{\mathrm{d}},$ and Δf are tracking errors for pitch angle, turbine speed, tip-speed ratio, turbine power and grid frequency respectively.

The error model (22)–(25) is valid for constant β_{d} and ω_{d}, defined in (12) and (13), respectively. These quantities are constants, if the wind speed and loads P_{la} and P_{l} are constants.

Error model (22)–(25) represents a cascade system, where the deviation of the turbine power from the desired one in (24) is driven by the blade pitch angle and turbine speed tracking errors, defined in (22) and (23), respectively.

The turbine power converges to the desired one and the control aim (8) is reached provided that the tracking errors for blade pitch angle and turbine speed defined in (22), (23) converge to zero. Both equations (22) and (23) represent exponentially stable dynamics and the control aims (6) and (7) are reached.

Finally, the equation for frequency deviation (25) represents a stable dynamics since $a_g > 0$ driven by exponentially convergent input $\tilde{P} + \varepsilon_t$, where ε_t is exponentially vanishing term, and the frequency regulation aim (5) is reached.

The stability can be proved and the transient bound on the tracking errors can be obtained using the following Lyapunov function $Q = \frac{1}{2}\tilde{\beta}^2 + \frac{J}{2}\tilde{\omega}^2 + \frac{1}{2}\Delta f^2$.

Notice that implementation of the controller (17)–(21) requires measurements of the frequency deviation Δf and wind speed V. The convergence rate of the feedforward speed control loop can be improved via introduction of the proportional feedback term driven by the mismatch $\tilde{\omega}$ in (21). This results in additional negative term in the error model (23) which improves the convergence rate.

Notice that classical feedforward $K\omega^2$ controller, which does not require wind speed measurements can also be applied to the generator torque control action T_{g} in (21), see for example Fleming (2016). Slower convergence is expected at lower wind speeds and for larger pitch angles due to wind speed dependent and restricted region of attraction in the speed control loop (Stotsky 2016b). This in turn results in larger tracking errors and deterioration of the performance in the coordinated APC service, since the desired power is delivered by the turbine when both quantities turbine speed and blade pitch angle converge to the desired values.

5.1 Simulation Results

Validated model of the wind turbine, described in Stotsky (2014) is used for simulations.

Time chart of the turbine active power control is presented in Fig. 6, where measured wind speed is plotted in the first subplot. The load estimated via algorithm (16) is
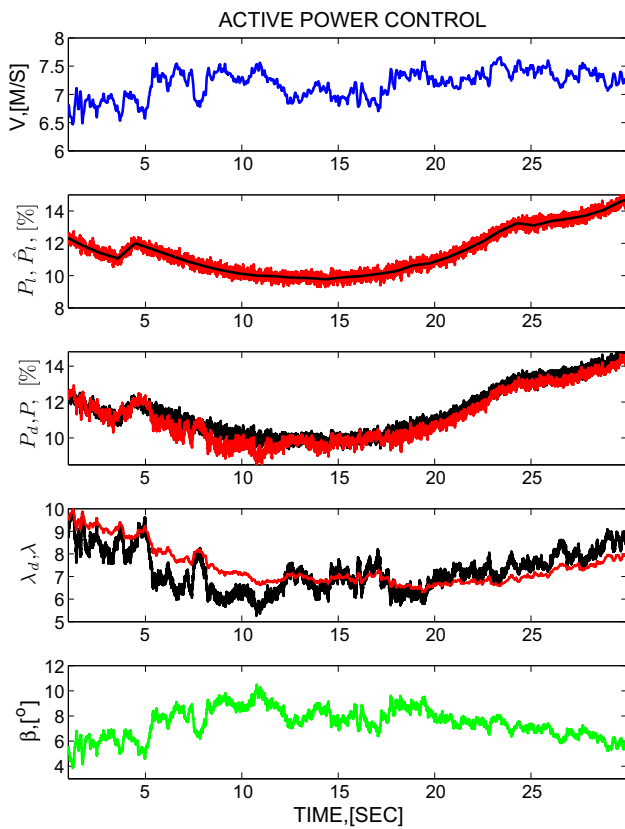
Fig. 6 Time chart of turbine active power control. The first subplot shows measured wind speed. The second subplot shows grid load estimation, where actual and estimated load are plotted with black and red lines, respectively. The third subplot shows normalized desired and actual turbine power (plotted with black and red lines, respectively). Desired and actual tip-speed ratio are plotted in the fourth subplot with black and red lines, respectively. Finally, the blade pitch angle is plotted in the fifth subplot (Color figure online)

plotted with a red line in the second subplot, where actual load is plotted with a black line. Requested and actual turbine power are plotted with black and red lines, respectively, in the third subplot. Requested and actual tip-speed ratio are plotted with black and red lines, respectively, in the fourth subplot. Finally, blade pitch angle is plotted in the fifth subplot. Frequency variations in SMG associated with APC are plotted with a red line in Fig. 7, where a black line represents time chart of the frequency without control with corresponding load trajectory plotted with a black line in the second subplot of Fig. 6.

6 Conclusion

This paper describes new robust wind turbine functionality, which reduces the effects of wind power and load variability in the frequency regulation. Namely, new wind turbine control architecture is developed is this paper for
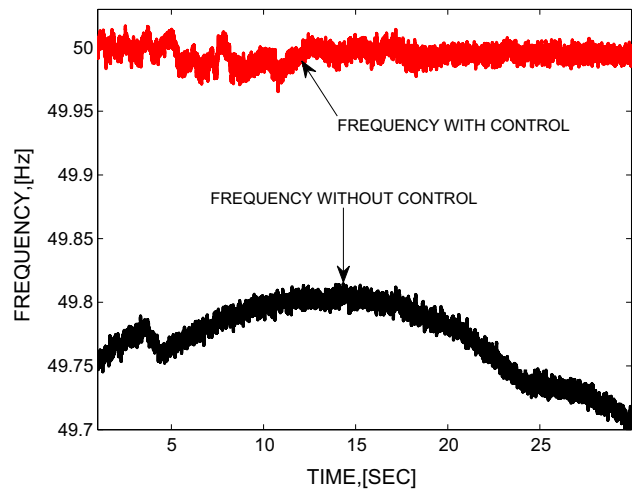

Fig. 7 Time chart of the grid frequency is plotted with a red line for Active Power Control shown in Fig. 6. The black line represents time chart of the frequency without control, where load trajectory is plotted with a black line in the second subplot of Fig. 6 (Color figure online)

high-performance frequency regulation in SMG. Proper coordination of pitch and speed control loops delivers desired power from wind turbine to the grid compensating for wind power variations in the frequency control loop. The impact of load variations is reduced via integration of the load observer driven by the frequency deviation in the wind turbine APC.

The performance of the frequency regulation can be further improved by adding anticipatory capability in the frequency control loop, taking into account LIDAR preview wind speed and direction (Stotsky et al. 2013) as well as load and weather forecast information (Berkel 2013).

Appendix: A Tool-Kit for Discrete-Time Input Estimation Algorithms

Problem Statement

Consider the following system :

$$x_k = ax_{k-1} + \underbrace{z_{k-1}}_{\text{known input}} - \underbrace{d + \xi_{k-1}}_{\text{unknown input}} \quad (26)$$

where x_k is measurable output of the system, z_k is known input, d is unknown constant input to be estimated, ξ_k is unmeasurable zero mean white Gaussian noise, $k = 1, 2, ...$ The system parameter $0 < a < 1$ is known.

The problem is to find estimator for unknown constant input d, using measurements of the system output x_k.

A Simple Data-Driven Estimator

Data-driven estimator $\hat{d}$ for unknown input d can be written as follows:

$$\hat{d}_k = \left\{ a^k x_0 + \sum_{j=0}^{k-1} a^{k-j-1} z_j - x_k \right\} \frac{(1-a)}{(1-a^k)} \qquad (27)$$

This estimator is suitable for tracking of unknown time varying input d_k. Accuracy of estimation is associated with the following estimation error

$$\hat{d}_k - d = -\frac{(1-a)}{(1-a^k)} \sum_{j=0}^{k-1} a^{k-j-1} \xi_j \qquad (28)$$

which is sufficiently small if a is close to one.

Notice that the estimator (27) provides better performance compared to the performance of the simplest estimation technique, which follows directly from (26) $\hat{d}_k = z_{k-1} + a x_{k-1} - x_k$.

Notice also that estimator (27) is a discrete-time counterpart of continuous time estimator proposed in Stotsky and Kolmanovsky (2002), which is widely used in automotive applications. Discrete-time estimators similar to (27) can also be found in Ljung (1999).

Least Squares Estimator

Description of the Estimator

Equation (26) can be written in the following form:

$$y_k = \varphi_k d + \zeta_k \qquad (29)$$

where $y_k = x_k - a^k x_0 - \sum_{j=0}^{k-1} a^{k-j-1} z_j$ is the synthetic output, $\varphi_k = -\frac{(1-a^k)}{(1-a)}$ is the regressor, d is unknown parameter, and ζ_k is input noise associated with the noise ξ_k.

Introduction of the following model

$$\hat{y}_k = \varphi_k \theta_k \qquad (30)$$

for system (29) together with minimization of the following performance index $E_k = \sum_{j=1}^{k} w_j (y_j - \hat{y}_j)^2$ with respect to the parameter θ_k yields:

$$\theta_k = \left[\sum_{j=1}^{k} w_j \varphi_j^2 \right]^{-1} \sum_{j=1}^{k} w_j \varphi_j y_j \qquad (31)$$

where w_j is a weighting sequence. Assigning weighting factor to one in step k and to λ_0 in the previous steps the least squares estimate (31) is written in the following recursive form:

$$\gamma_k = \frac{\gamma_{k-1}}{\lambda_0 + \gamma_{k-1} \varphi_k^2}, \quad \gamma_0 > 0 \qquad (32)$$

$$\theta_k = \theta_{k-1} + \gamma_k \varphi_k (y_k - \theta_{k-1} \varphi_k) \qquad (33)$$

where $0 < \lambda_0 < 1$ is a forgetting factor. Notice that stability of the system (29), (30), (32) and (33) is proved in Stotsky (2013) for general case.

Limiting Form of the Estimator

Least squares estimator (32), (33) can be simplified for implementation via substitution the limiting form of the gain $\gamma_\infty = (1-\lambda_0)(1-a)^2$ in (33) as follows :

$$\theta_k = \theta_{k-1} - (1-\lambda_0)(1-a)(1-a^k)(y_k - \theta_{k-1}\varphi_k) \qquad (34)$$

The estimator is driven by the synthetic output $y_k = x_k - a^k x_0 - \sum_{j=0}^{k-1} a^{k-j-1} z_j$ associated with the system (26).

Substituting regressor in (34) and neglecting for simplicity the transient component associated with a^k the error model is presented in the following form:

$$\tilde{\theta}_k = \lambda_0^k \tilde{\theta}_0 - (1-\lambda_0)(1-a) \sum_{j=1}^{k} \lambda_0^{j-1} \zeta_{k-j+1} \qquad (35)$$

where $\tilde{\theta}_k = \theta_k - d$ is estimation error, $k = 1, 2....$ Accuracy of estimation is determined (after some transient) by the second term in Eq. (35), which is associated with the noise. This term can be made sufficiently small, if forgetting factor λ_0 is close to one. The same factor λ_0 determines the convergence rate of estimated parameter θ_k to its true value d, and the convergence is slow, if λ_0 is close to one. In other words the choice of the forgetting factor represents a tradeoff between the tracking performance of fast varying d_k and accuracy of estimation associated with amplification of input noise.

The estimator (34) may provide better performance compared to simple estimator (27) provided that the parameter λ_0 is chosen properly.

Notice that algorithm (34) is a discrete-time counterpart of the continuous time turbine inertia moment estimation algorithm described in Stotsky et al. (2013), see also Stotsky and Egardt (2013).

References

Aho, J., et al. (2012). A tutorial of wind turbine control for supporting grid frequency through active power control. In *2012 American control conference, Fairmont Queen Elizabeth, Montreal*, June 27–June 29 (pp. 3120–3131).

Berkel, F., et al. (2013). Load-frequency control, economic dispatch and unit commitment in smart microgrids based on hierarchical model predictive control. In *52-nd IEEE CDC, Florence*, Dec 10–13 (pp. 2326–2333).

Fan, L. (2017). *Control and dynamics in power systems and microgrids*. Boca Raton, FL: CRC Press, Taylor & Francis.

Farhangi, H. (2010). The path of the smart grid. *IEEE Power & Energy Magazine*, *8*, 18–28.

Fleming, P., et al. (2016). Effects of power reserve control on wind turbine structural loading. *Wind Energy*, *19*, 453–469.

Ljung, L. (1999). *System identification: Theory for the user*. Upper Saddle River, NJ: Prentice-Hall.

Pao, L., & Johnson, K., (2009). A tutorial on the dynamics and control of wind turbines and wind farms. In *Proceedings of American control conference, St. Louis, MO*, 10–12 June (pp. 2076–2089).

Pipattanasomporn, M., et al. (2014). Load profiles of selected major household appliances and their demand response opportunities. *IEEE Transactions on Smart Grid*, *5*(2), 742–750.

Stotsky, A. (2013). Harmonic regressor: Robust solution to least-squares problem. *Proceedings of the Institution of Mechanical Engineers Part I: Journal of Sytems and Control Engineering*, *227*(8), 662–668.

Stotsky, A. (2014). Wind turbine model validation: Fusion of simulation and measurement data. *Proceedings of the Institution of Mechanical Engineers Part I: Journal of Systems and Control Engineering*, *228*(9), 734–737.

Stotsky, A. (2016a). Towards accurate estimation of fast varying frequency in future electricity networks: The transition from model-free methods to model-based approach. *Proceedings of the Institution of Mechanical Engineers Part I: Journal of Systems and Control Engineering*, *230*(10), 1164–1175.

Stotsky, A. (2016b). Nonlinear speed and yaw control for wind turbine powered vessels. *Proceedings of the Institution of Mechanical Engineers Part I: Journal of Systems and Control Engineering*, *230*(3), 255–265.

Stotsky, A., & Egardt, B. (2013). Data-driven estimation of the inertia moment of wind turbines: A new ice detection algorithm. *Proceedings of the Institution of Mechanical Engineers Part I: Journal of Sytems and Control Engineering*, *227*(6), 552–555.

Stotsky, A., Egardt, B., & Carlson, O. (2013). An overview of proactive wind turbine control. *Energy Science & Engineering*, *1*, 1–10.

Stotsky, A., & Kolmanovsky, I. (2002). Application of input estimation techniques to charge estimation and control of automotive engines. *Control Engineering Practice*, *10*, 1371–1383.

Ulbig, A., Borsche, T., & Andersson, G. (2014). Impact of low rotational inertia on power system stability and operation. arXiv:1312.6435v4 [math.OC]

Undrill, J., (2010). Power and frequency control as it relates to wind-powered generation, PhD Thesis, Ernest Orlando Lawrence Berkeley National Laboratory

Wang-Hansen, M., Josefsson, R., & Mehmedovic, H. (2012). Frequency controlling wind power: Modeling of control strategies. *Elforsk Report*, *12*, 43.

Yingcheng, X., & Nengling, T. (2011). Review of contribution to frequency control through variable speed wind turbine. *Renewable Energy*, *36*, 1671–1677.